

EFFECTS OF CORROSION ON TENSION STIFFENING AND CRACKING BEHAVIOUR OF REINFORCED ENGINEERED CEMENTITIOUS COMPOSITETIES AND CONCRETE

L. LI^{*}, E. CHEN^{*}

^{*} Huazhong University of Science and Technology, School of Civil and Hydraulic Engineering, Wuhan, China
e-mail: lilei_@hust.edu.cn

Key words: ECC, Rebar corrosion, Tension stiffening, Distributed optical fiber sensors

Abstract: As a kind of ductile fiber-reinforced cementitious composite, Engineered Cementitious Composite (ECC) has great crack width control ability and improved durability. However, there are only limited studies on the durability of steel reinforced ECC (R/ECC) members. This makes the service life quantification of R/ECC members lack of research data. The present study investigates the interaction behaviour between steel rebar and ECC after corrosion exposure. Results from four R/ECC and four reinforced concrete (RC) ties with the dimension of 75×75×600 mm and corrosion levels up to about 5% were reported herein. Corrosion-induced cracks were recorded during accelerated corrosion tests. After corrosion, the corroded ties were tested under uniaxial tension together with the uncorroded ties. Steel strain distributions of specimens during tension were monitored by distributed optical fiber sensors (DOFS) to examine the stress transfer mechanism between rebar and matrix. The impacts of steel corrosion on the tension-stiffening behaviour of R/ECC specimens were compared with those of RC ones. It was found that the corrosion-induced cracking degree in ECC was much smaller than that in concrete. Moreover, corrosion improved tension-stiffening effect in all R/ECC ties and decreased in all RC ties from the load-average strain curves. The number of transverse major cracks in corroded R/ECC ties was kept similar as in the uncorroded tie, but the microcracks number decreased. In the group of RC ties, the transverse major cracks were only seen in the uncorroded specimen whereas several secondary cracks emerging from longitudinal cracks appeared in corroded specimens. Further, DOFS data displayed that steel reinforcement in ECC generally exhibited more uniform deformation than that in concrete. The strain distributions in corroded R/ECC ties were not changed apparently, and the steel strains in the corroded R/ECC ties are slightly larger than those in the uncorroded R/ECC tie at similar average corrosion level. This implies that bond strength can be well maintained in uncorroded R/ECC. The distance of strain peaks in corroded RC ties increased compared to that in the uncorroded RC tie, which reflected a decrease of bond strength in corroded RC ties for the investigated corrosion levels. The results from this study reveal that R/ECC members are less impaired by steel corrosion compared to concrete.

1 INTRODUCTION

Steel corrosion is one of the major causes affecting the durability of reinforced concrete (RC) structures. Corrosion can decrease the

cross-sectional area of steel bars, generate concrete cracking and spalling due to volumetric expansion of corrosion products, and change the bond property between concrete and rebar. These effects comprehensively endanger the durability and structural performance of RC structures under

both serviceability and ultimate limit states^[1]. According to a lot of previous studies, it is known that the alteration of bond behaviour in corroded members is greatly dependent on the cover cracking degree caused by corrosion expansion^[2]. Most researchers^[3,4] carried out pull-out tests of corroded specimens to study the effect of corrosion on bond behavior. However, their bond length and boundary conditions are different with those in full-scale structural members. Therefore, a limited number of studies^[5] performed direct tensile tests on corroded reinforced concrete tie elements (i.e., concentrically reinforced concrete prisms or cylinders). They are much longer than pull-out specimens, and can simulate the tensile zone of RC members better than pull-out specimens. In the tensile tests of RC tie elements, the tension-stiffening phenomenon is particularly of interest, as well as crack characteristics (crack spacing and crack width) and stress distributions of steel, concrete and the interface. In previous studies^[6] on the tensile behavior of RC tie elements subjected to various degree of corrosion, it has been generally found that corrosion decreased the tension-stiffening effect, leading to fewer load cracks and wider load crack width.

Engineered Cementitious Composite (ECC), as a type of high-performance fiber-reinforced cementitious composite, has superior crack control ability due to multiple cracking principle and exhibits high ductility, thus overcoming the brittleness of conventional concrete^[7]. Previous studies have shown that ECC could restrain corrosion-induced cracking, suppress cover spalling and decrease the decay degree of structural performance of corroded beams^[8]. Regarding the bond behavior in corroded R/ECC, Hou et al.^[9] reported the effect of corrosion on the bond performance between steel bar and ECC through pull-out tests. They found that the bond strength in specimens with large bond length (112mm) was nearly unchanged for corrosion levels up to 15% in mass loss, and even increased for smaller bond length at corrosion levels less than 10%. This indicated that the delaying of corrosion cracking in ECC greatly improved the resistance to bond

degradation. However, how the rebar corrosion affects the tension-stiffening behavior of corroded R/ECC and stress transfer between ECC and rebar is unclear.

Moreno et al.^[10] have studied the tension stiffening effect in R/ECC ties (without corrosion) and examined the steel strain distribution through strain gauges placed along the embedded bar. They showed that ECC could carry loads greater than the yield load of steel bar leading to a higher load carrying capacity than steel bar and RC up to tensile strains of approximately 1~2%. But the ductility (i.e. deformation at failure) of R/ECC ties was lower than that of RC due to the localized early strain hardening of steel bar in ECC. When steel corrosion occurs, ECC would suffer less damage caused by corrosion expansion than concrete. Accordingly, the influence of corrosion on the tension-stiffening and stress transfer in R/ECC ties which is related to corrosion cracking would be probably different with that in RC ties.

In order to reveal the effect of steel corrosion on the tension-stiffening behavior of R/ECC, this study conducted tensile tests on R/ECC ties which had been subjected to accelerated corrosion. Moreover, to better understand the stress transfer mechanism between ECC and steel bar, distributed optical fiber sensors (DOFS) based on Optical Frequency Domain Reflectometer (OFDR) and Rayleigh scattering, which have a high spatial resolution of 1mm, were arranged along the longitudinal ribs of steel bar to monitor steel strain distribution and evolution during the loading process. The impacts of steel corrosion on the tension-stiffening behaviour of R/ECC were compared with those of RC by analyzing the load-average strain curve, load-induced cracking pattern, and steel strain distribution.

2 EXPERIMENT DESCRIPTION

2.1 Specimens preparation

Eight reinforced prismatic specimens with a cross-section of 75mm×75mm and 600mm in length were prepared in this study, including four R/ECC ties and four RC ties. They are

labelled as R/ECC-0, R/ECC-1, R/ECC-2, R/ECC-3, RC-0, RC-1, RC-2 and RC-3. Each specimen was centrally reinforced with one HRB400E rebar with the diameter of 12mm and length of 900mm, leading to a reinforcement ratio of 2.01%. The steel bars used in this study had an elastic modulus of 200GPa, yield strength of 433MPa, ultimate strength of 587MPa and ultimate strain of 0.183. To avoid localized corrosion near the ends of prisms, epoxy resin was applied on the end parts of steel bar surface, as shown in Fig.1. The optical fiber sensors adopted in this study was a tightly-sheathed fiber sensor with 0.9mm in diameter including the core, cladding and coating layer. Before casting, two fiber sensors were bonded along the two longitudinal ribs to monitor the steel strain distribution in the following tensile tests.

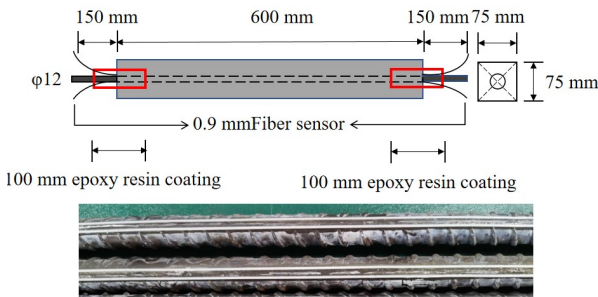


Figure 1: Sketch of the tie specimen and optical fiber sensor arrangement.

The ECC used in this study has a water to binder ratio of 0.22, consisting of ordinary Portland cement with Grade 42.5, class F fly ash, 0.1mm~0.25mm quartz sand, polycarboxylate superplasticizer and 2% by volume polyvinyl alcohol (PVA) fiber which has a length of 12mm, a diameter of 40 μ m, and tensile strength of 1250MPa. Concrete used in the study has a water to cement ratio of 0.55, consisting of silica sand, gravel (maximum aggregate size of 16mm), and Grade 42.5 cement. The mixture proportions of ECC and concrete are shown in Table 1. Three ECC dog-bone specimens and four ECC cubes with 70mm in length were prepared to determine their tensile properties and compressive strength. Three concrete cubes with 150mm in length were cast to determine the compressive strength of concrete.

Table 1 (a): Mix proportions of concrete (kg/m³)

Cement	Silica sand	Water	Gravel
500	600	275	1025

Table 2 (b): Mix proportions of ECC (kg/m³)

Cement	Silica sand	Water	Fly ash	PVA	SP
278	278	305	1110	26	2

The dog-bone and cubic specimens were demolded within 3 days and then cured for 28 days under standard curing conditions. The concrete had an average compressive strength of 36.1MPa and the ECC had an average compressive strength of 37.8 MPa. ECC tensile tests were carried out under displacement control with a loading rate of 0.2mm/min. An LVDT was used to record the deformation of the center 80mm part of the specimen. Dimensions and tensile test setup of the dog-bone ECC specimen is shown in Fig.2.

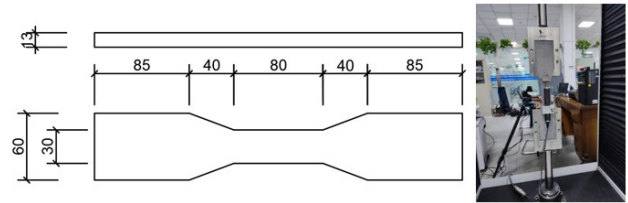


Figure 2: Dimensions and tensile test setup of ECC (unit in mm).

2.2 Accelerated corrosion test

Impressed current method was used in this study to accelerate the steel corrosion process of the tie specimens. A tank containing 3.5% sodium chloride was set up on the top side of the specimen. The positive electrode of the power supply was connected to the steel bar, and the negative electrode was connected to a stainless-steel net. The current was set as 0.08A, which gave the current density as 424 μ A/cm² for the exposed area of steel in the study. The corrosion test setup is shown in Fig.3.

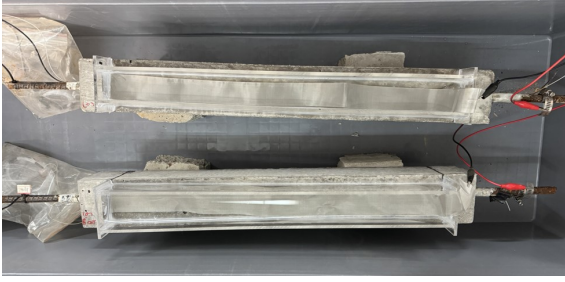


Figure 3: Accelerated corrosion test setup of tie specimens.

The designed mass loss of steel investigated in this study included 1%, 3%, and 5%. The required corrosion time corresponding to these designed corrosion levels was first calculated by Faraday's law with a constant corrosion current being assumed. Three tie specimens in each group (R/ECC-1, R/ECC-2, R/ECC-3 and RC-1, RC-2, RC-3) were subjected to current for the calculated corrosion time corresponding to 1%, 3% and 5% corrosion level respectively. During the accelerated corrosion test, the voltage and current was continuously monitored. It was found that the current could not achieve the set value at first few days because the resistance of the specimens was too high and the voltage capacity of the power supply is only 60V. Therefore, the theoretical mass loss from Faraday's law based on the measured current was calculated later. Moreover, the actual steel mass loss was also measured after the tensile tests of corroded specimens. For this purpose, the initial mass of all steel bars was also weighed beforehand.

2.3 Tensile test setup

After the corrosion test, all specimens were tested on a 1000kN MTS universal test machine in monotonic tension with displacement control. The loading rate was set as 0.6mm/min in the elastic stage and 2mm/min after steel yielding. Two LVDTs were used to measure the deformation of the central 500mm part of specimens and their average value was taken. The test setup is shown in Fig.4.

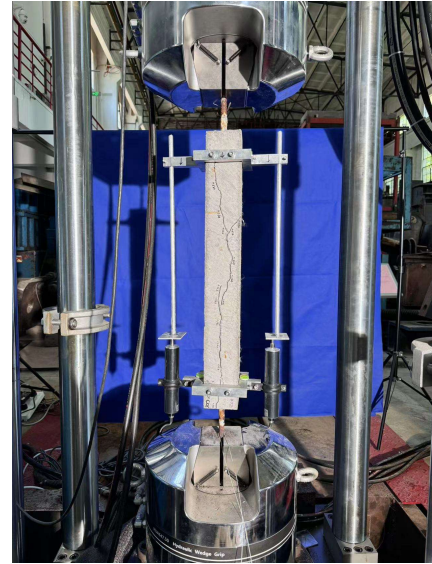


Figure 4: Test set up of tie specimens.

3 RESULTS AND DISCUSSIONS

3.1 Uniaxial tensile test results of ECC

The tensile stress-strain curves of ECC dog-bone specimens are shown in Fig.5. All specimens exhibited multiple cracking and strain hardening behavior, but the ultimate strain varied among different specimens. This may be caused by the difference of fiber distribution quality in different specimens.

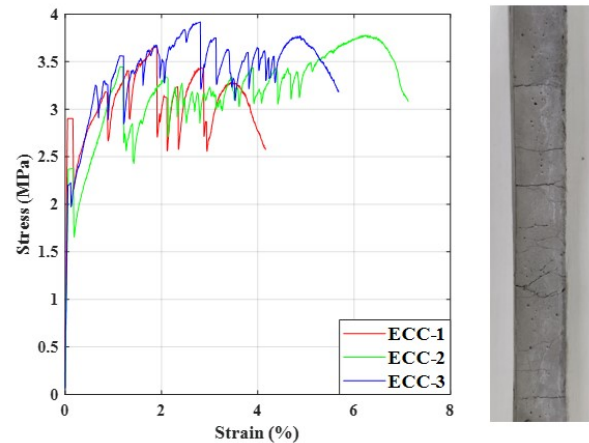


Figure 5: Stress-strain curve and multiple cracking of ECC from the side view.

3.2 Results from corrosion tests

3.2.1 Corrosion level

The theoretical mass loss of steel bars was determined by Faraday's law shown in Eq. (1),

$$\Delta m_F = MI t / Fz \quad (1)$$

where Δm_F represents the mass loss (g) from Faraday's law, M is the molar mass of iron (55.8 g/mol), I is the corrosion current (Amps), t is the corrosion time (s), F is Faraday's constant (96487 A/s) and z is the valency of iron (taken as 2). The corrosion current I was taken as the output current of the power supply registered by the data logger, and corrosion time t was taken as the period when the power supply was applied. It should be noted that the current efficiency may not be 100% for the steel corrosion process and the corrosion initiation time was also not the beginning time of current applying. This causes the actual mass loss is different with the theoretical value. Therefore, the actual mass loss was also determined by subtracting the weight of steel bar which was cleaned after uniaxial tensile test from the weight prior to corrosion.

The designed mass loss, theoretical mass loss from Faraday's law and actual mass loss of each specimen are given in Table 2. It can be seen that the theoretical mass loss of all specimens except R/ECC-3 is larger than the actual mass loss. This is reasonable since the corrosion time is overestimated as mentioned before.

3.2.2 Corrosion-induced crack pattern

All corroded tie specimens underwent various degrees of corrosion-induced cracking under the expansion of internal corrosion products. The crack pattern was recorded after the corrosion tests and crack width along the crack path was measured at an interval of 50mm by a crack detector. The crack pattern and widths of the most severe damaged face for each specimen is shown in Fig.6. From Fig. 6, the crack pattern for ECC and concrete group specimens was similar, i.e., a major longitudinal crack above the steel bar generated. However, it is obvious that ECC greatly restrained the corrosion cracking development. Under similar corrosion level, the crack widths in R/ECC specimens were much smaller than those in RC specimens. It

should be noted that the crack trajectory shown in Fig. 6 was traced by a marker next to the real crack to clearly display the crack pattern, so the thickness of the crack trajectory was not the actual crack width. Most crack widths of ECC cover were less than 0.1mm, but the maximum crack width was still large, which was 0.218mm in ECC-C3.00 and 0.109 mm in ECC-C5.00. This may be due to that the amount of fiber in these cross-sections was not adequate. The average crack width was calculated and given in Table 2. It can be seen that the average corrosion-induced crack width increases as the corrosion level increases. The maximum average corrosion-induced crack width of the three R/ECC specimens was only 65 μ m which was less than one-sixth of the maximum average crack width (404 μ m) in RC specimens.

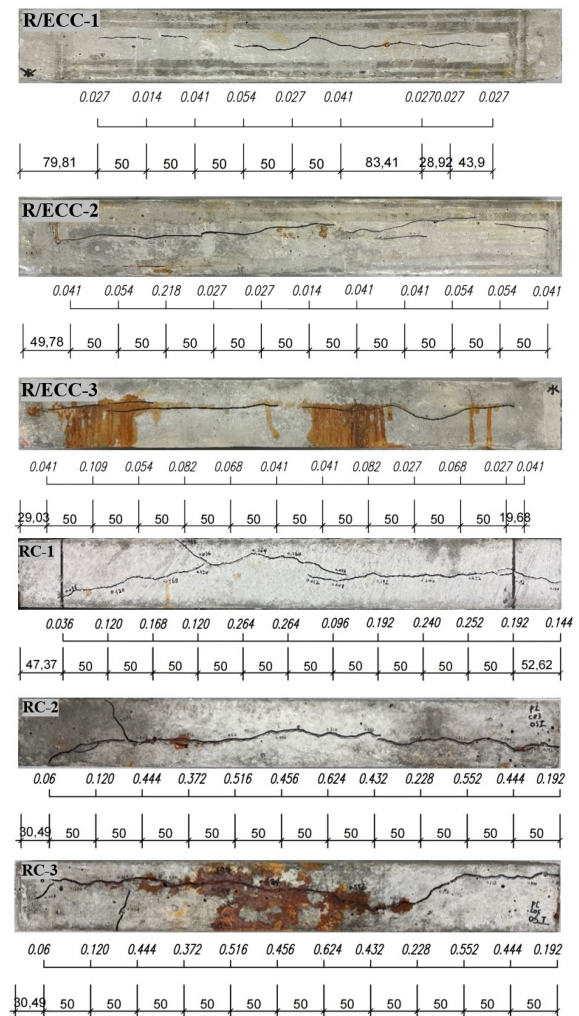


Figure 6: Mapping and widths of corrosion-induced cracks of corroded tie specimens

Table 2: Mass loss and average corrosion crack width of the tie specimens

Specimen	Mass loss percentage (%)			Average corrosion crack width (mm)
	Design	Theoretical	Actual	
R/ECC-0	0.00	0.00	0.00	0.000
R/ECC-1	1.00	1.03	0.45	0.032
R/ECC-2	3.00	2.95	2.58	0.056
R/ECC-3	5.00	4.83	5.19	0.065
RC-0	0.00	0.00	0.00	0.000
RC-1	1.00	3.35	0.44	0.174
RC-2	3.00	5.19	5.14	0.404
RC-3	5.00	7.02	5.77	0.397

3.3 Tensile test results

3.3.1 Crack pattern of tie specimens after tension

The crack patterns of the most damaged faces of specimens are displayed in Fig.7. In the group of all ECC specimens, two dominant transverse cracks were generated and numerous microcracks also appeared. It can also be seen that the primary crack pattern has almost no difference except that the number of microcracks in the uncorroded R/ECC is more than that in the corroded specimens. However, in the group of concrete specimens, the crack pattern of corroded specimens is obviously different with that of the uncorroded specimen. There were two major transverse cracks going through the cross section in the uncorroded RC tie, which was absent in corroded RC ties. Instead, several cracks in corroded RC ties developed from the existing corrosion cracks. These cracks are referred to as secondary cracks in the following.

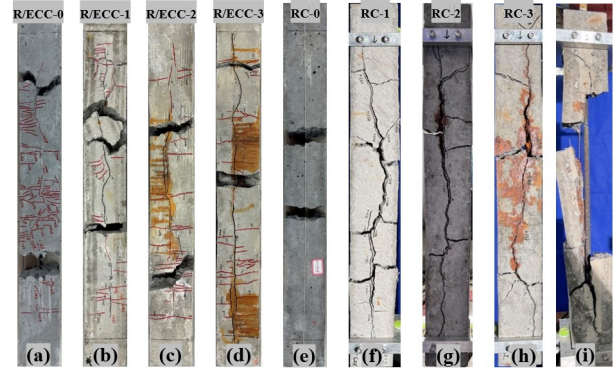
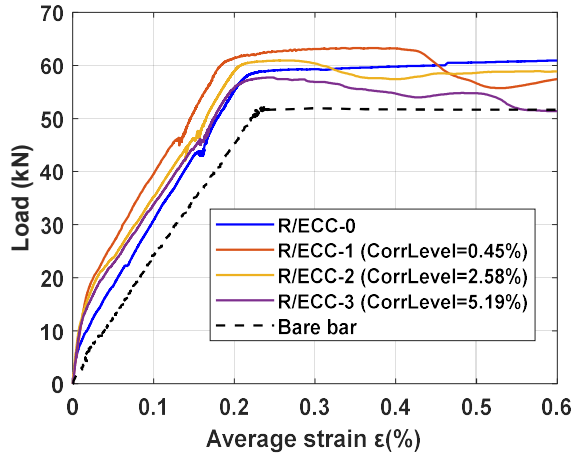


Figure 7: Crack pattern of uncorroded and corroded tie specimens under tension

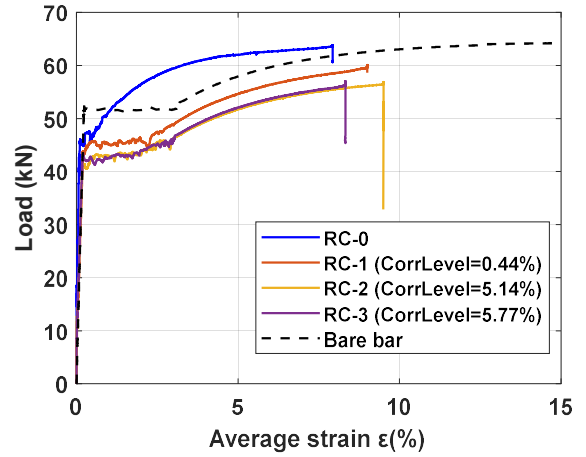
3.3.2 Load-average strain curve

The load-average strain curves of all the tie specimens at earlier stage are shown in Fig. 8 and the full response are given in Fig. 9. The average strain was obtained from the readings of two LVDTs. The load-strain curve of the bare steel bar is also plotted in the figures to examine the tension-stiffening effect contributed by ECC or concrete. From Fig. 8a, it can be seen that the tension-stiffening effect in corroded R/ECC ties is greater than that in the uncorroded one. In addition, the specimen R/ECC-1 with the smallest corrosion level of 0.45% increased the tension stiffening effect most. From the load-average strain curve of the uncorroded RC tie in Fig. 8b, this specimen has unexpectedly higher stiffness and smaller yielding strain. The authors believed that this is due to the twisting effect of the end grips acting on this specimen which was caused by the wrong gripping sequence of the two ends (noted during the test).

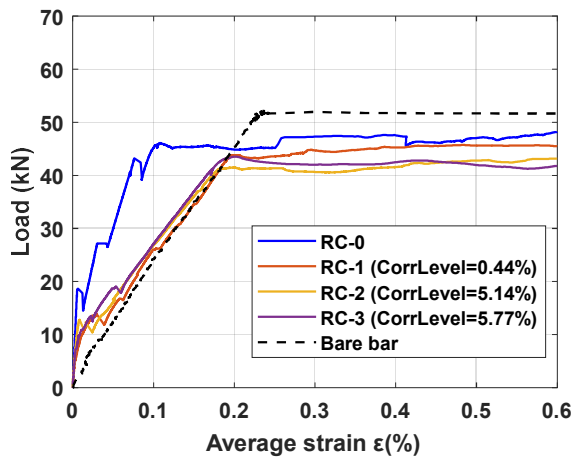
From Fig. 9, the ultimate force of uncorroded R/ECC and RC is similar to that of bare steel bar. With the effect of steel corrosion in R/ECC ties, the ultimate force almost kept similar for R/ECC-1 and R/ECC-2, and only decreased slightly (about 4.1%) for R-ECC-3 with the highest corrosion level. The ultimate force of corroded RC ties decreased by about 10.8% for RC-2 and RC-3. The ultimate ductility of all specimens would not be discussed here since the measuring range of LVDT was exceeded in some specimens.



(a)

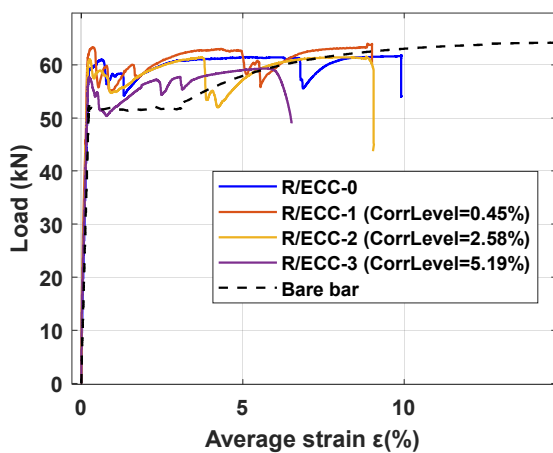


(b)



(b)

Figure 8: Load-average strain curves of R/ECC and RC ties at earlier stage



(a)

Figure 9: Full response of load-average strain curves of R/ECC and RC ties

3.3.3 Strain distribution evolution of steel bars measured by DOFS

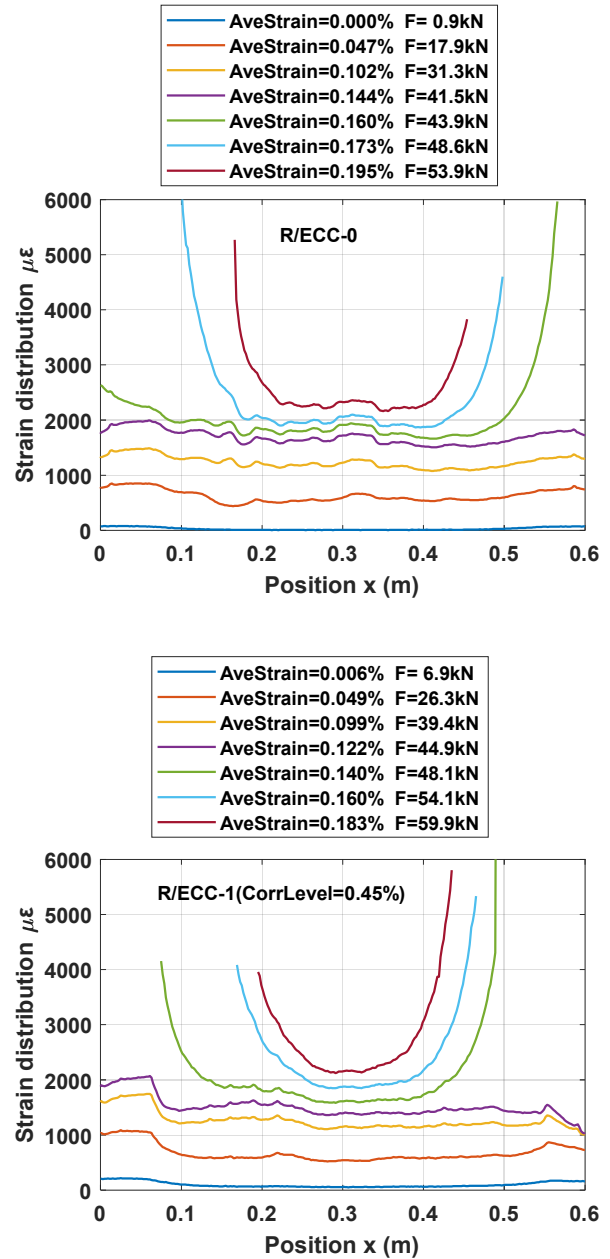
Figure 10 displays the steel strain distribution of each specimen at selected load levels and average strains. It should be noted that results from the specimen RC-3 were not available due to some operation error. In addition, abnormal data were removed in the plots. Since abnormal values appear more frequently at later loading stages for most specimens, only results up to average strain of about 0.2% are shown. The strain distributions near the two ends were not discussed as epoxy resin was coated there for the purpose of avoiding localized corrosion in the ends, and the strain transferring effect of fiber sensor near the ends may also cause the results near the two ends difficult to interpret.

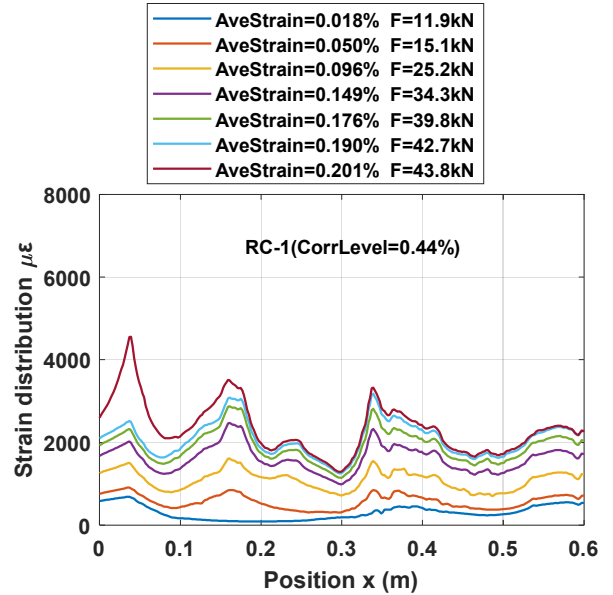
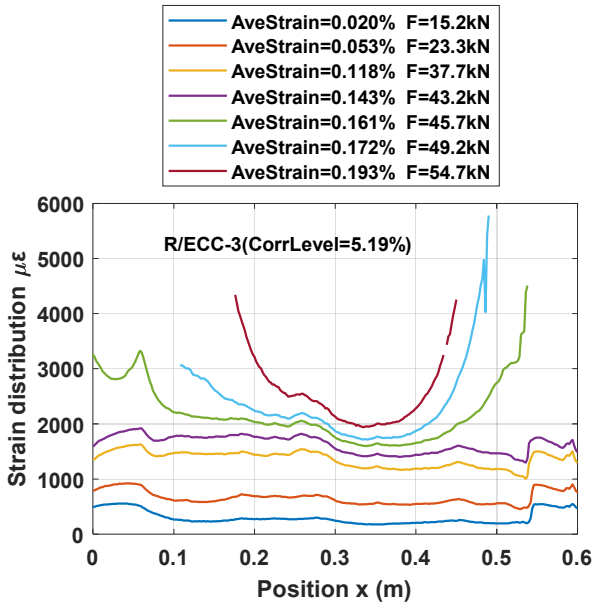
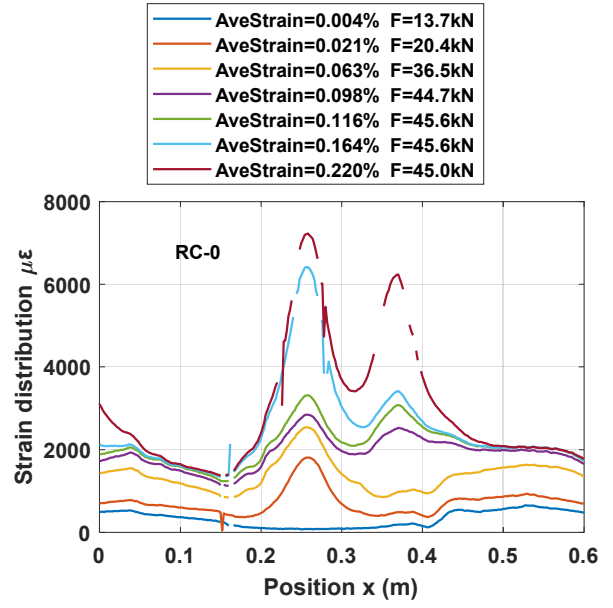
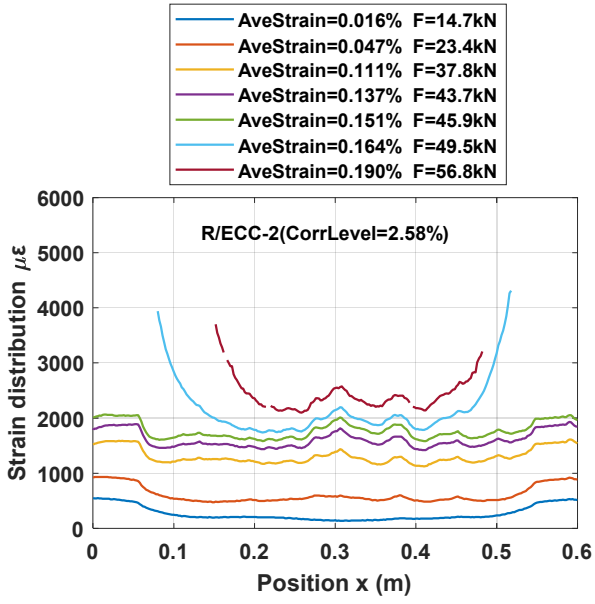
In general, the strain distributions of steel in R/ECC ties are almost uniform with small variation, and no obvious strain peaks can be seen for both uncorroded and corroded ties. For RC ties, there are obvious two strain peaks showing on the plots at very early stage. In the uncorroded RC tie (i.e. RC-0), the positions of the two peaks ($x=0.26\text{m}$ and 0.37m) correspond to the two major transverse cracks well. For the corroded specimens, two peaks appear at the position of 0.16m and 0.34m in RC-1 and at the position of 0.23m and 0.4m in RC-2. Therefore, the distance of the two strain

peaks increases in the corroded RC ties compared to the uncorroded RC tie. This can indicate the decrease of bond strength which results in a larger transfer length.

Figure 11 compares the steel strain distribution of all specimens at average strain of about 0.1%. It should be noted that since the data acquisition frequency for different specimens is different, the average strain of each specimen for comparison is a little different. The values of the specimen RC-0 were not quantitatively compared with others due to their inaccuracy caused by the twisting of the end grip, which has been mentioned before. However, showing the tendency of RC-0 and the position of strain peaks is also meaningful. Overall, the strain distribution pattern keeps similar in R/ECC ties, and strain values increase slightly in the corroded R/ECC ties compared to those in the uncorroded R/ECC tie for similar average strain. By comparing the strain values of RC-1 and RC-2, the peak value is much higher in RC-2 which has greater corrosion level.

The lack of strain peaks in R/ECC ties reflects the strain compatibility of steel and ECC. Once cracking occurs in concrete, the force would be carried by the steel alone at the cracked position, which results in strain concentration in steel. However, after cracking occurs in ECC, it can still carry force due to the fiber bridging. As a result, no steel strain concentration takes place. It should be noted that strain distribution of steel after significant yielding or hardening could not be examined in this study due to the measuring range and abnormal value problem.





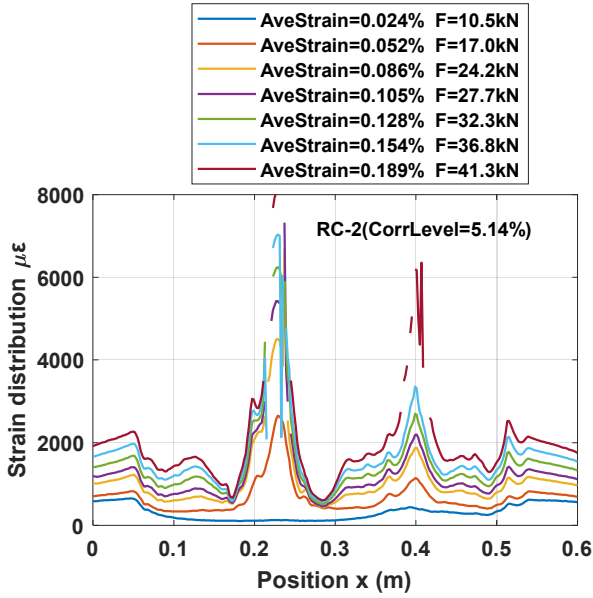


Figure 10: Steel strain distributions of each specimen at selected load levels and average strains

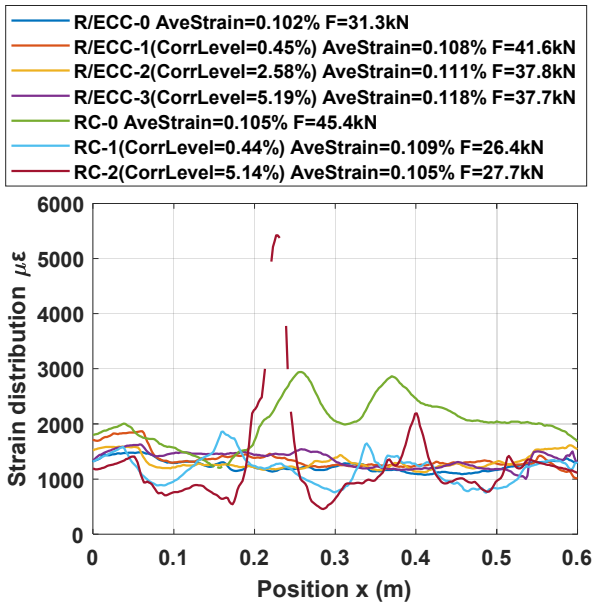


Figure 11: Comparison of steel strain distribution of each specimen at average strain of about 0.1%

4 CONCLUSIONS

Tension stiffening behaviour of uncorroded and corroded R/ECC and RC ties has been investigated in this study with distributed optical fiber sensors. The following conclusions can be drawn from the results.

- ECC suffered less corrosion-induced

cracking than concrete at similar corrosion level. The average corrosion crack width was only 65μm in R/ECC, and 404μm in RC under similar corrosion level of about 5%.

- Corroded R/ECC ties had slightly higher tension-stiffening effect under the investigated corrosion levels, while the tension-stiffening effect decreased in corroded RC ties.
- Steel strain distributions was almost uniform in R/ECC, for both uncorroded and corroded tie specimens. However, strain peaks appear early in RC specimens which reflecting the steel strain concentration at concrete cracks. In addition, the distance of strain peaks in corroded RC ties was longer than that in the uncorroded RC tie.

From the results above, R/ECC could better sustain the adverse effect of steel corrosion than RC. This will help to extend the service life of structures under corrosion environment. Specimens with higher corrosion levels need to be further studied.

REFERENCES

- [1] Avadh, K., Jiradilok, P., Bolander, J. E. and Nagai, K., 2021. Direct observation of the local bond behavior between corroded reinforcing bars and concrete using digital image correlation. *Cement and Concrete Composites*. 123.
- [2] Moccia F., Ruiz M. F., Muttoni A., 2021. Spalling of concrete cover induced by reinforcement. *Engineering Structures*. 237.
- [3] Mancini G., Tondolo F., 2014. Effect of bond degradation due to corrosion - a literature survey. *Structural Concrete*. 15(3): 408-418.
- [4] Ma Y., Guo Z., Wang L., Zhang J., 2017. Experimental investigation of corrosion effect on bond behavior between reinforcing bar and concrete. *Construction*

and Building Materials. 152: 240-249.

- [5] Giordano L., Mancini G., Tondolo F., 2011. Reinforced Concrete Members Subjected to Cyclic Tension and Corrosion. *Journal of Advanced Concrete Technology*. 9(3): 277-285.
- [6] Imperatore S., Rinaldi Z., Drago C., 2017. Degradation relationships for the mechanical properties of corroded steel rebars. *Construction and Building Materials*. 148: 219-230.
- [7] Li, V. C. and Leung, C. K., 1992. Steady-state and multiple cracking of short random fiber composites, *Journal of Engineering Mechanics*. 118(11), 2246-2264.
- [8] Sahmaran, M., Li, V C. and Andrade, C., 2008. Corrosion Resistance Performance of Steel-Reinforced Engineered Cementitious Composite Beams, *ACI Materials Journal*. 105(3):243-250.
- [9] Hou L., Liu H., Xu S., Zhuang N., Chen D., 2017. Effect of corrosion on bond behaviors of rebar embedded in ultra-high toughness cementitious composite. *Construction and Building Materials*. 138: 141-150.
- [10] Moreno D. M., Trono W., Jen G., Ostertag C., Billington S. L., 2014. Tension stiffening in reinforced high performance fiber reinforced cement-based composites. *Cement and Concrete Composites*. 50: 36-46.